AD-A071 283 IBM RESEARCH LAB SAN JOSE CALIF F/G 7/4
COLLISON-INDUCED OPTICAL DOUBLE RESONANCE II,(U)
JUL 74 R L SHOEMAKER, S STENHOLM, R G BREWER N00014-72-C-0153
UNCLASSIFIED RJ-1422

| OF |
AD
A071283

END
DATE
FILMED
8-79
DDC

IBM Research

COLLISION-INDUCED OPTICAL DOUBLE RESONANCE II

R. L. Shoemaker/S. Stenholm
Richard G. Brewer

July 30, 1974

RJ 1422

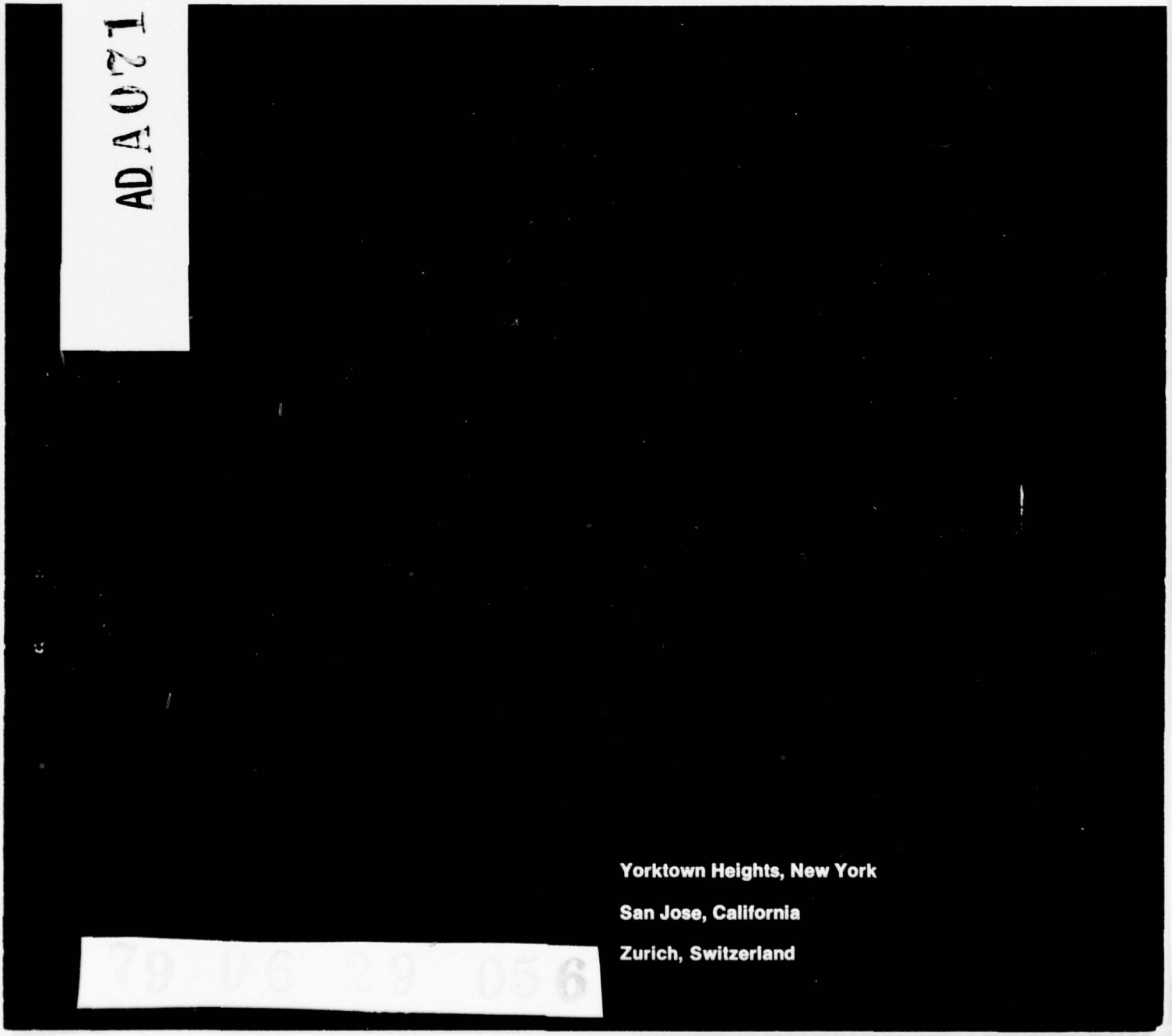

Yorktown Heights, New York

San Jose, California

Zurich, Switzerland

Limited Distribution Notice

This report has been submitted for publication elsewhere and has been issued as a Research Report for early dissemination of its contents. As a courtesy to the intended publisher, it should not be widely distributed until after the date of outside publication.

Copies may be requested from:
IBM Thomas J. Watson Research Center
Post Office Box 218
Yorktown Heights, New York 10598

DATA SHEET

PHOTOGRAPH

THIS SHEET

IF

LEVEL

1

INVENTORY

AD A071283

DDC ACCESSION NUMBER

RJ-1422, Dtd. 30 July '74
(#21968)

DOCUMENT IDENTIFICATION

DISTRIBUTION STATEMENT A
Approved for public release;
Distribution Unlimited

DISTRIBUTION STATEMENT

Accession For
NTIS GRA&I
DDC TAB
Unannounced
Justification
Per FL-88(R79-0857)
By On file
Distribution/
Availability Codes
Dist | Avail and/or special
A

DISTRIBUTION STAMP

DDC
RECEIVED
JUL 17 1979
D

DATE ACCESSIONED

DDC FILE COPY

79 06 29 056

DATE RECEIVED IN DDC

PHOTOGRAPH THIS COPY

RJ 1422 (#21968)
July 30, 1974
Physics (General)

COLLISION-INDUCED OPTICAL DOUBLE RESONANCE II*†

R. L. Shoemaker*
S. Stenholm**
Richard G. Brewer

IBM Research Laboratory
San Jose, California 95193

ABSTRACT: In a previous paper, we demonstrated that a set of new resonances can accompany the conventional infrared Lamb-dip or double resonance transitions in CH_3F gas. These satellite lines have a different origin from the primary resonances even though they are similar in intensity and line width. The traditional double resonance, for example, requires that a molecule interact simultaneously with two radiation fields, causing a transition from an initial to a final state through an intermediate level. *Here, the double resonance concept is extended to the situation of two coherently driven optical transitions that do not share a common level but are coupled by molecular collisions that tip the angular momentum vector while preserving the molecular velocity and rotational energy.* Thus, velocity selective population changes are communicated from one transition to another through collisions. Collision-induced double resonance is observed with Stark tuning as a series of sharp lines, free of Doppler broadening and can be explained in the same order of perturbation theory as the ordinary double resonance experiment. Each satellite corresponds to a specific level structure involving one or more collision-induced transitions among the space quantized M states. Virtually all characteristics of these satellite resonances, either in Lamb-dip or double resonance experiments, are in agreement with the theory presented.

---

*First presented at the Quantum Electronics Conference VIII, San Francisco, June 10-13, 1974; S. Stenholm, R. G. Brewer and R. L. Shoemaker.

†Work sponsored in part by the U.S. Office of Naval Research under contract No. N00014-72-C-0153.

*Present address: Optical Sciences Center, University of Arizona, Tucson.

**On leave from the Research Institute for Theoretical Physics, University of Helsinki, 00170 Helsinki 17, Finland.

1. INTRODUCTION

Nonlinear resonance phenomena that utilize laser light have provided unique spectroscopic techniques for the study of atoms and molecules. Examples are the Lamb-dip and the double resonance effect where a molecule interacts simultaneously with two radiation fields. The fields may be of the same frequency and propagate in opposite directions as in the Lamb-dip, or be of different frequency, Ω_1 and Ω_2, and move in the same direction as in the double resonance effect. In either case, the two monochromatic light waves saturate two narrow velocity groups within the Doppler distribution. When these merge into one velocity group either due to tuning of the molecular level structure or the laser frequency, this group interacts simultaneously with both fields and exhibits a sharp resonance that is free of Doppler broadening. This class of nonlinear optical effects is now well known and extends the radio frequency double resonance methods developed in molecular beam[1] and optical pumping experiments.[2]

In a previous paper,[3] we demonstrated that a set of new resonances can accompany the ordinary Lamb-dip[4] or optical double resonance transitions.[5-8] These satellite lines, which have not been discussed before, have a different origin from the primary resonances even though they are similar in intensity and line width. As an illustration, Fig. 1 shows a double resonance spectrum for an infrared transition of the symmetric top molecule $^{13}CH_3F$ which is tuned by means of a d.c. Stark field for the experimental arrangement shown in Fig. 2(c). The ordinary double resonances, lines (c) and (e), correspond to the molecular level structure of Fig. 2(a) where the transition proceeds from an initial to

a final state through an intermediate level. The remaining lines, the satellites, display a different tuning behavior and correspond to the level structure of Fig. 2(b). Here, the two transitions involved do not share a common level but are coupled by molecular collisions rather than optically. In a bimolecular encounter, the partially saturated molecules are transferred from one level to another without an appreciable velocity change. Thus, velocity-selective population changes are communicated from one transition to another through collisions.

The relevant collision mechanism, first discussed by Anderson,[9] is the electric dipole-dipole force of two $^{13}CH_3F$ molecules. The anisotropic part of this interaction can tip the angular momentum vector without changing the longitudinal molecular velocity or the rotational energy. Recent photon echo experiments[10] on $^{13}CH_3F$ reveal, in fact, that the average velocity jump per collision is only 200 cm/sec. It has not been realized until now, however, that even if the velocity changes but little in a collision, a molecule may reorient easily, going from an initial space quantized state M to another of the same J state. This circumstance leads to the newly discovered double resonance, characterized by a sharp resonant tuning behavior, free of Doppler broadening, and with an intensity comparable to the traditional double resonance signal. For the same reasons, Lamb-dip spectra also are found to exhibit collision-induced satellite lines. These effects thus add another dimension to nonlinear optical spectroscopy and offer a new way of examining molecular collisions, particularly those involving reorientation.

This article presents further observations and a theory of collision-induced Lamb-dip and optical double resonance phenomena not contained in our earlier communication.[3] The basic interpretation that the two optical transitions are coupled by collisions, rather than optically, is fully confirmed by our theoretical findings in virtually all details. Optical coupling mechanisms have been explored also, but according to our estimates are too weak to be seen (Appendix C).

It should be noticed that collision-induced optical double resonance resembles four level microwave double resonance,[11] where collisional relaxation among molecular rotational states has been investigated. There are, however, two significant differences. First, the optical work is velocity sensitive and the more energetic collisions needed to produce a rotational energy jump can also lead to a velocity smearing which would manifest itself in the line width. The microwave experiments do not supply this information because the entire Doppler lineshape is monitored.

Second, in microwave double resonance, the four levels involved are usually all coupled to one another by collisions. The infrared experiment is simpler because radiation and collisions induce different transitions (see Fig. 2(b)). This arises from the vibrational decay being considerably slower than orientational and rotational relaxation. Hence, the upper and lower level pairs essentially remain collisionally isolated from each other. Data analysis is therefore straightforward for the optical case and the extraction of collision cross sections is facilitated.

Recently, molecular collisions which induce an inversion[12] in NH_3 and a rotational quantum jump[13] in CO_2 have been noted in other forms of optical double resonance. These were observed as single resonances corresponding to one collision induced quantum jump but are manifestations of the same double resonance condition even though they were not observed as satellite lines accompanying the primary double resonance signals. Each satellite line, on the other hand, corresponds to a specific level configuration where the collisionally coupled M states involve one or more quantum jumps. Another distinction is that pronounced velocity smearing can occur when the collisions involve a larger energy transfer than the angular momentum tipping process described here.

2. THEORY

2.1 Basic Equations

The double resonance experiment is performed in the configuration shown in Fig. 2(c). Two cw lasers are locked to a fixed frequency difference $\Omega_1 - \Omega_2$ and their light enters the Stark cell from the same direction. We write the field in the cell

$$E_x(z,t) = E_1 \cos(\Omega_1 - kz) + E_2 \cos(\Omega_2 - kz) \tag{2.1}$$

where we neglect the differences between the propagation vectors $k_i = \Omega_i/c$ $(i=1,2)$. This is a good approximation because the frequency difference is in the r.f. region.[14] A moving molecule will experience a field obtainable from (2.1) when its instantaneous position $z(t)$ along the beam direction is inserted.

The two fields can resonantly drive two transitions, shown in Fig. 2(b), where c and a are sublevels of the excited state and b,d of the ground state. In the dipole approximation, the levels are optically coupled by

$$H_I = -\mu_x E_x(z,t) \tag{2.2}$$

and the selection rules are such that

$$\langle a|\mu_x|b\rangle = \mu_{ab} \neq 0, \quad \langle c|\mu_x|d\rangle = \mu_{cd} \neq 0$$

$$\langle a|\mu_x|d\rangle = \langle b|\mu_x|c\rangle = 0 \ . \tag{2.3}$$

We want the equation of motion for the four level system in Fig. 2(b) including collisional coupling between a-c and b-d. A straightforward generalization of the treatment of Ref. 15 leads to the equation of motion for the velocity dependent density matrix

$$i\frac{\partial\rho(v)}{\partial t} = i\Lambda(v) + [H,\rho(v)] - \frac{i}{\tau}\rho(v) + i\int\frac{dv'}{T(v')}[\Pi(v,v') - \delta(v-v')]\rho(v') \ , \tag{2.4}$$

where the diagonal matrix Λ is the steady state rates at which molecules enter the optically active levels. The decay constant τ is the duration of the interaction assumed to be dominated by the molecular transit time across the laser beam and is taken to be equal for all density matrix elements. The last term of Eq. (2.4) represents the effects of collisions

on the density matrix; T(v) is the average time between collisions. In general the collision operator Π is complicated (see Appendix B and below), but for the present purpose it reduces to the term containing κ in Eq. (2.10).

The collision kernel $\Pi(v,v')$ is a matrix operator in the indices of the density matrix. It can cause three qualitatively different features. We will discuss the influence of each one for the double resonance experiments on the symmetric top molecule CH_3F.

(a) The phase of the complex off-diagonal elements, Π_{ab} say, cause phase shifts of the molecular oscillators. These are observed as collision shifts and broadenings of the spectral lines as in the ordinary Lorentz treatment.[16] In dilute molecular systems, collisions affect the vibrational transitions very weakly; in particular Schmidt, Berman and Brewer[10] show that phase-changing collisions have a negligible influence on CH_3F.

(b) The integration in the collision operator derives from the velocity changes induced by the molecular scattering process. In Ref. 10 it is shown that an average velocity jump is $\Delta u \simeq 200$ cm/sec which corresponds to a frequency of $\Delta\nu \approx k\Delta u \approx 10^5$ Hz. Because this is of the order of the observed molecular line width, most encounters take place without removing the molecule from the velocity group interacting with the field. In the simplified treatment to be presented we neglect velocity

changes, i.e., $\Pi(v,v') \propto \delta(v - v')$; an extension allowing collisional smearing of the velocity is discussed in Appendix B.

(c) The collisions are allowed to change the M state of the molecule. We assume the mixing of the optically coupled (vibrational states) to be negligible but allow reorientation of the angular momentum. This manifests itself as a coupling between the states a-c and b-d. The result is a transfer of velocity dependent populations from one transition to the other. As the two transitions are driven by different frequencies we expect the stochastic distribution of the collision times to make the coherent coupling average to zero (i.e., there is no transfer of off-diagonal elements between the two transitions). This presumes that the influence of off-resonance driving (Ω_2 on a-b and Ω_1 on c-d) is negligible. The possibility that off-resonant driving could be observed in a double resonance experiment is discussed in Appendix C, and it is shown to be too weak.

We introduce the collision broadened line width

$$\gamma = \frac{1}{\tau} + \frac{1}{T} , \tag{2.5}$$

with (1/T) being the contribution from all types of collisions (for simplicity we assume the same T for all levels). The fraction of the line width due to reorientation is

$$\kappa = \left[\frac{1}{\tau} + \frac{1}{T}\right]^{-1} \left(\frac{1}{T}\right)_{\text{reorientation}} . \qquad (2.6)$$

With power broadening, γ determines the observed line width and κ determines the strength of the new resonances. Collisions that change the angular momentum J are not monitored in the present experiments but contribute to γ. The transition frequencies are

$$\omega_{ij} = (E_i - E_j)/\hbar \qquad (2.7)$$

with E_i the energy of $|i\rangle$. In general four velocity groups are excited, viz.

$$kv = \Omega_1 - \omega_{ab} , \quad kv' = \Omega_2 - \omega_{cd} \qquad (2.8)$$

$$kv'' = \Omega_1 - \omega_{cd} , \quad kv''' = \Omega_2 - \omega_{ab} . \qquad (2.9)$$

In the double resonance only one pair will be of interest, e.g. (2.8), where the field E_1 is in resonance with transition a-b and E_2 with c-d. We can then consider one field for each transition only, as opposed to both fields driving both transitions.

For a certain choice of selection rules (vide infra) each field can interact with one of the transitions only.

2.2 Calculation of the Density Matrix

We first consider the equations for the transition a-b only. With the simplifications discussed in the previous section these equations are

$$i\dot{\rho}_{bb} = i(\lambda_b - \gamma\rho_{bb}) + 2\alpha_1 \cos(\Omega_1 t - kz)(\rho_{ba} - \rho_{ab}) + i\gamma\kappa_{bd}\rho_{dd} \qquad (2.10)$$

$$i\dot{\rho}_{ab} = \omega_{ab}\rho_{ab} - i\gamma\rho_{ab} - 2\alpha_1 \cos(\Omega_1 t - kz)(\rho_{bb} - \rho_{aa}) \qquad (2.11)$$

and the corresponding equations for ρ_{aa} and ρ_{ba}. We use the notation

$$\alpha_1 = \mu_{ab}E_1/2\hbar \qquad (2.12)$$

and introduce molecules in the state $|b\rangle$ at the rate λ_b as defined in Eq. (2.4) (and λ_a for level $|a\rangle$). The collisions are assumed to transfer population, not coherence, and γ is the decay rate due to all processes depleting $|b\rangle$ including transfer to $|d\rangle$.

We remove the rapidly oscillating component of the off-diagonal element[17] by setting

$$\rho_{ab} = \tilde{\rho}_{ab}\, e^{-i(\Omega_1 t - kz)} \qquad (2.13)$$

and perform the rotating wave approximation to obtain from (2.11)

$$\tilde{\rho}_{ab} = \frac{\alpha_1}{(\Delta_1 + kv) - i\gamma}\, n_{ba} \qquad (2.14)$$

where

$$\Delta_1 = \omega_{ab} - \Omega_1 \,. \qquad (2.15)$$

From (2.8) and the equation for ρ_{aa} we obtain

$$n_{ba} \equiv \rho_{bb} - \rho_{aa} = \frac{2i\alpha_1}{\gamma} (\tilde{\rho}_{ab} - \tilde{\rho}_{ba}) + \kappa_{bd}\rho_{dd} - \kappa_{ac}\rho_{cc} + \frac{\lambda_b - \lambda_a}{\gamma} . \quad (2.16)$$

From these equations we find that

$$\tilde{\rho}_{ab} - \tilde{\rho}_{ba} = \frac{2i\alpha_1\gamma}{(\Delta_1 + kv)^2 + \Gamma_1^2} \left[\kappa_{bd}\rho_{dd} - \kappa_{ac}\rho_{cc} + \frac{\lambda_b - \lambda_a}{\gamma} \right] \quad (2.17)$$

where

$$\Gamma_1^2 = \gamma^2 + 4\alpha_1^2 \quad (2.18)$$

is the power broadened line width.

The populations ρ_{dd} and ρ_{cc} have to be obtained from the equations for the transition c-d. In analogy with Eqs. (2.10)-(2.16) we obtain

$$\tilde{\rho}_{cd} \equiv e^{i(\Omega_2 t - kz)} \rho_{cd} = \frac{\alpha_2}{(\Delta_2 + kv) - i\gamma} n_{dc} \quad (2.19)$$

where

$$\alpha_2 = \mu_{cd} E_2 / 2\hbar \quad (2.20)$$

and

$$\Delta_2 = \omega_{cd} - \Omega_2 . \quad (2.21)$$

Further we obtain

$$n_{dc} \equiv \rho_{dd} - \rho_{cc} = \frac{2i\alpha_2}{\gamma} (\tilde{\rho}_{cd} - \tilde{\rho}_{dc}) + \kappa_{bd}\rho_{bb} - \kappa_{ac}\rho_{aa} + \frac{\lambda_d - \lambda_c}{\gamma} . \quad (2.22)$$

In order to insert ρ_{dd} and ρ_{cc} into (2.17) we solve Eqs. (2.19) and (2.22) with the collisions neglected. This corresponds to a perturbation expansion in κ_{bd} and κ_{ac}, which is justified in the present case because κ is small. We obtain

$$n_{dc} = \frac{\lambda_d - \lambda_c}{\gamma}\left[1 - \frac{4\alpha_2^2}{(\Delta_2 + kv)^2 + \Gamma_2^2}\right] \tag{2.23}$$

where

$$\Gamma_2^2 = \gamma^2 + 4\alpha_2^2 \ . \tag{2.24}$$

In the same approximation we can obtain

$$\rho_{dd} + \rho_{cc} = \frac{\lambda_d + \lambda_c}{\gamma} \tag{2.25}$$

and solve for

$$\rho_{dd} = \frac{\lambda_d}{\gamma} - \frac{\lambda_d - \lambda_c}{\gamma}\ \frac{2\alpha_2^2}{(\Delta_2 + kv)^2 + \Gamma_2^2} \tag{2.26}$$

$$\rho_{cc} = \frac{\lambda_c}{\gamma} + \frac{\lambda_d - \lambda_c}{\gamma}\ \frac{2\alpha_2^2}{(\Delta_2 + kv)^2 + \Gamma_2^2} \tag{2.27}$$

giving for the double resonance part of (2.17) the expression

$$\tilde{\rho}_{ab}^{(1)} - \tilde{\rho}_{ba}^{(1)} = -\frac{4i\alpha_1\alpha_2^2(\kappa_{bd} + \kappa_{ac})(\lambda_d - \lambda_c)}{[(\Delta_1 + kv)^2 + \Gamma_1^2][(\Delta_2 + kv)^2 + \Gamma_2^2]}\ , \tag{2.28}$$

where we have omitted terms which fail to display sharp double resonance behavior. We note that the polarization given by (2.28) is strongly enhanced when $\Delta_1 = \Delta_2$, because this allows the same velocity group to satisfy both resonance conditions of the denominator.

Proceeding from Eqs. (2.19) and (2.22) we can in an identical way derive the double resonance contribution to the element ρ_{cd} in the form

$$\tilde{\rho}_{cd}^{(1)} - \tilde{\rho}_{dc}^{(1)} = - \frac{4i\alpha_2\alpha_1^2(\kappa_{bd} + \kappa_{ac})(\lambda_b - \lambda_a)}{[(\Delta_1 + kv)^2 + \Gamma_1^2][(\Delta_2 + kv)^2 + \Gamma_2^2]} \tag{2.29}$$

exhibiting a resonance behavior identical with that of (2.28).

2.3 The Absorption Measurement

The polarization induced in molecules by the field (2.1) is

$$P(z,t) = N[\mu_{ab}(\rho_{ab} + \rho_{ba}) + \mu_{cd}(\rho_{cd} + \rho_{dc})] \ . \tag{2.30}$$

The energy absorbed in the sample is proportional to

$$W = \overline{\langle E(z,t)\dot{P}(z,t)\rangle_{vel}} \tag{2.31}$$

where the bar denotes a time average and $\langle\ \rangle_{vel}$ a velocity average. Introducing ρ_{ab} from (2.13) and ρ_{cd} from (2.19) into (2.30) we obtain

$$W = \frac{1}{2} N \left\langle [\mu_{ab} E_1 \Omega_1 (\tilde{\rho}_{ab} - \tilde{\rho}_{ba}/1) + \mu_{cd} E_2 \Omega_2 (\tilde{\rho}'_{cd} - \tilde{\rho}_{dc}/1)] \right\rangle \quad . \tag{2.32}$$

From (2.28) and (2.29) we obtain the velocity average

$$\left\langle \frac{1}{[(\Delta_1 + kv)^2 + \Gamma_1^2][(\Delta_2 + kv)^2 + \Gamma_2^2]} \right\rangle_{vel}$$

$$= \frac{1}{ku\sqrt{\pi}} \int e^{-x^2/k^2u^2} \frac{dx}{[(\Delta_1 + x)^2 + \Gamma_1^2][(\Delta_2 + x)^2 + \Gamma_2^2]}$$

$$= \frac{1}{ku\sqrt{\pi}} \; e^{-\Delta_1^2/k^2u^2} \frac{\pi(\Gamma_1 + \Gamma_2)}{\Gamma_1\Gamma_2[(\Delta_1 - \Delta_2)^2 + (\Gamma_1 + \Gamma_2)^2]} \quad . \tag{2.33}$$

Inserting (2.28), (2.29) with (2.33) into (2.32) we find for the absorption

$$W = - \frac{4\sqrt{\pi}\, N\alpha_1^2\alpha_2^2}{ku\Gamma_1\Gamma_2} \; e^{-\Delta_1^2/k^2u^2} \frac{(\Gamma_1 + \Gamma_2)}{[(\Delta_1 - \Delta_2)^2 + (\Gamma_1 + \Gamma_2)^2]} \cdot$$

$$\times (\kappa_{ac} + \kappa_{bd})[\hbar\Omega_1(\lambda_d - \lambda_c) + \hbar\Omega_2(\lambda_b - \lambda_a)] \quad , \tag{2.34}$$

where Δ_1 equals Δ_2 in the exponent at resonance. This is the final result to be compared with the experiments. In our approximation the result is proportional to the average collisional reorientation rate $\gamma' = \frac{1}{2}\gamma(\kappa_{ac} + \kappa_{bd})$.

This result is to be compared with the expression for the ordinary double resonance which is given in Appendix A for easy comparison.

2.4 Lamb-dip Measurements

It is straightforward to generalize these considerations to a Lamb-dip experiment.[4] We take a standing wave

$$E_x(z,t) = 2E \cos \Omega_1 t \cos kz = E \cos(\Omega_1 t - kz) + E \cos(\Omega_1 t + kz) \quad (2.35)$$

instead of (2.1) and find that the calculations remain the same with $(\Omega_2 t - kz)$ replaced by $(\Omega_1 t + kz)$. The parameters α_1 and α_2 now contain the same field E but still have different transition matrix elements. The double resonance contribution to the polarization (2.29) now reads

$$\tilde{\rho}^{(1)}_{cd} - \tilde{\rho}^{(1)}_{dc} = - \frac{4i\alpha_2\alpha_1^{\,2}(\kappa_{bd} + \kappa_{ac})(\lambda_b - \lambda_c)}{[(\omega_{ab} - \Omega_1 + kv)^2 + \Gamma_1^{\,2}][(\omega_{cd} - \Omega_1 - kv)^2 + \Gamma_2^{\,2}]} \quad (2.36)$$

and the final result after Doppler averaging is

$$W = - \frac{4\sqrt{\pi}\, N\alpha_1^{\,2}\alpha_2^{\,2}}{ku\Gamma_1\Gamma_2} \exp[-(\omega_{ab} - \Omega_1)^2/k^2u^2]$$

$$\times \frac{\frac{1}{4}(\Gamma_1 + \Gamma_2)}{\left[\left(\frac{\omega_{ab} + \omega_{cd}}{2} - \Omega_1\right)^2 + \frac{1}{4}(\Gamma_1 + \Gamma_2)^2\right]} (\kappa_{ac} + \kappa_{bd})\hbar\Omega_1(\lambda_d - \lambda_c + \lambda_b - \lambda_a) \,. \quad (2.37)$$

There now occurs a resonance at

$$\Omega_1 = \frac{1}{2}(\omega_{ab} + \omega_{cd}) \tag{2.38}$$

with line width $\frac{1}{2}(\Gamma_1 + \Gamma_2)$, in contrast to the previously found line width $(\Gamma_1 + \Gamma_2)$. This derives from the two conditions

$$\omega_{ab} = \Omega_1 - kv\ , \qquad \omega_{cd} = \Omega_1 + kv \tag{2.39}$$

being satisfied for the same velocity group (see (2.8)). Now, however, the conditions

$$\omega_{ab} = \Omega_1 + kv\ , \qquad \omega_{cd} = \Omega_1 - kv \tag{2.40}$$

corresponding to (2.9) are satisfied simultaneously, thus enhancing the signal by a factor of two. Two symmetrically situated velocity groups at

$$kv = \pm(\omega_{ab} - \Omega_1) \tag{2.41}$$

are involved, in contrast to the ordinary Lamb-dip which involves only one group at zero velocity. The measured intensity is, consequently, twice the result given in (2.37).

3. APPARATUS

3.1 Double Resonance

The experimental arrangement[8] schematically given in Fig. 2(c) is displayed in detail in Fig. 3. It consists of two laser beams which are collinear and propagate in the same direction through a precision Stark cell, containing a $^{13}CH_3F$ gas sample, before striking a photodetector. The signals are monitored with phase sensitive detection using small amplitude Stark modulation. The radiation is provided by two CO_2 lasers with identical construction for frequency stability.[18] Each operates cw with single frequency output, the power is about 1 W in each line, and oscillation on any one of 70 lines in the 9 and 10 μm bands is controlled by a rotatable grating at one end of the laser cavity. In this experiment, both lasers oscillate on the same line, the P(32) line of the 9 μm band at 1035.474 cm^{-1}.

Reproducible resonances are obtained by frequency locking one laser to the other. This is accomplished by monitoring their beat frequency $(\Omega_1 - \Omega_2)$ with a germanium-gold doped photodetector, and comparing it with an r.f. reference. A frequency to voltage converter produces an error signal that drives the cavity length of one of the lasers by means of a piezoelectric. Long term stability of 1/100,000 can be achieved in the difference frequency $(\Omega_1 - \Omega_2)$ which could be set in the range 10 to 50 MHz.

Both laser beams are expanded to 1 cm diameter with the aid of a telescope in order to increase the molecular time of flight in the

transverse direction. The resulting power densities at the Stark cell are $\sim$1.2 and 0.4 W/cm^2. The beams are normally polarized perpendicular to the Stark field, imposing $\Delta M = \pm 1$ selection rules. However, parallel polarized light and the $\Delta M = 0$ selection rule are obtained by inserting a CdS half-wave plate in one or both beams.

The vibration-rotation transition of $^{13}CH_3F$ investigated was the fundamental ν_3 band line $(J,K) = (4,3) \rightarrow (5,3)$. It coincides within its 66 MHz Doppler-width with the P(32) CO_2 laser line. The double resonance spectrum, as will be seen, confirms the line assignment unambiguously and agrees with that of conventional infrared spectroscopy[19] where the K splitting is not resolved. The gas sample contained a 90% or more enrichment of $^{13}CH_3F$.

The optical Stark cell is made of components having optical tolerances and consists of two fused quartz disks that are 4 in. diam. × 3/4 in. thick, flat to $\pm 10^{-5}$ cm and coated on the inner surfaces with vacuum deposited aluminum. Separating the flats are fused quartz spacers whose thickness as determined by gage blocks is 0.60256 ± 0.00001 cm. Measurements of the Stark voltage are made with a digital voltmeter, checked against a standard, and accurate to 0.008%.

The Stark field is swept in steps and the double resonance spectrum recorded digitally by means of a small computer. This procedure facilitates signal averaging and data handling and allows a least squares fit of the lines to a Lorentzian lineshape, including an accurate

determination of the line centers and line widths. The spectrum of Fig. 1 shows an example of the computer plot. Alternatively, spectra may be obtained without a computer using a continuous Stark voltage sweep as in Figs. 4 and 5. For the dipole moment measurements, line positions are an average of forward and reverse sweeps and the zero voltage condition was tested by reversal of the power supply leads to the Stark cell.

3.2 Lamb-dip

This experiment requires only one CO_2 laser and resembles one of our earlier studies.[20] The incident beam, after passing through the Stark cell, is partially reflected ($\sim$8%) back upon itself by a BaF_2 optical flat. It is slightly misaligned in angle so as not to enter the laser cavity and disturb its operation. The remaining 92% of the incident beam is monitored with a photodetector and displays Lamb-dip resonances with Stark tuning.

4. EXPERIMENTS

4.1 Double Resonance

An optical double resonance spectrum of $^{13}CH_3F$ is shown in Fig. 1 when the optical selection rule is $\Delta M = \pm 1$. This constitutes the primary evidence for collision-induced optical double resonance. These lines appear as the molecular levels $|J,K,M\rangle$ in lower and upper vibrational states are tuned by an external electric field ε causing the first order Stark shift[21]

$$\Delta W_1 = -\mu\varepsilon MK/[J(J+1)] \ . \tag{4.1}$$

All of the lines of Fig. 1 satisfy the resonance condition

$$\Omega_1 - \Omega_2 = (m\Delta_\ell - n\Delta_u)\varepsilon \tag{4.2}$$

where m and n are integers and from (4.1) the Stark tuning rate $\Delta \equiv \Delta W_1/\varepsilon$ applies either to the lower or upper vibrational state. The strong lines (c) and (e) are the ordinary double resonances with the level structure of Fig. 2(a) and correspond to $\Delta M = 2$ intervals in the lower and upper levels, respectively.

The remaining lines (a, b, d and f) are the collision-induced resonances and correspond to the level configuration of Fig. 2(b) where the two transitions do not share a common level. Table I lists characteristics for each line of Fig. 1 where $(\Omega_1 - \Omega_2) = 30.008$ MHz and identifies the integers m and n in Eq. (4.2). Thus, line (a) involves two transitions whose upper levels are separated by a $\Delta M = 4$ interval while the lower levels are split by a $\Delta M = 2$ interval. The positions of the satellite lines are predicted on the basis of the Stark tuning rates Δ_ℓ and Δ_u obtained from the ordinary double resonance lines (c) and (e), and it is seen that the agreement with the observed values is good to 1/1000 or better. The accuracy of these predictions removes any doubt that the satellite lines are double resonances involving four levels, i.e., two transitions without a common level.

The line widths indicated in Table I are about 50x narrower than the 66 MHz Doppler width, but notice that the satellite lines are about twice the width of the three level double resonances, in agreement with Eq. (2.34) and Eq. (A.19). The fact that the two types of double resonance have about the same line width shows that the velocity is essentially preserved and supports the photon echo results.[10]

Other characteristics of Eq. (2.34) have been confirmed by experiment also. For example, by attenuating the intensity of either laser beam, it is seen that the collision-induced double resonance signal varies as $E_1^2 E_2^2$, in accord with the $\alpha_1^2 \alpha_2^2$ product of (2.34). The three level double resonance signals behave in the same way (see Eq. (A.19)). Furthermore, the anticipated linear pressure dependence is verified. Only at the lowest pressure is a quadratic dependence approached because then $\kappa \sim \gamma'/\gamma$ varies as N since the line width γ is dominated by the molecular time of flight τ across the laser beam.

4.2 Dipole Moments

In Table II similar data are presented for the case $(\Omega_1 - \Omega_2) = 40.039$ MHz and $\Delta M = \pm 1$ selection rules. The behavior generally reproduces Table I but is considered to be more accurate due to the higher beat frequency and narrower line widths. For this reason, permanent electric dipole moments for the ground and excited ν_3 vibrational states were obtained from these data and are given in Table III. These values were reported by us earlier in preliminary form (Ref. 8(b)) and they are in good

agreement with the values derived from molecular beam experiments[22] (ground state) and Stark tuned laser spectroscopy of Freund et al.[23] The slightly higher moment for J = 12 suggests the influence of rotational distortion.

4.3 Off-resonant Driving Mechanism

Another possible mechanism that could couple two transitions not having a common level is an off-resonant driving effect. This involves two distinct molecular groups, each in resonance with its own radiation field. If we consider, for example, that the field of frequency Ω_2 not only drives the transition c-d resonantly but also the transition a-b nonresonantly, an interference effect with a double resonance tuning behavior can occur, as explained in Appendix C. While such an effect reproduces some of the observed double resonance characteristics, it severely violates others. A dramatic example of disagreement with this mechanism is shown in Fig. 4 and the corresponding Table IV where the selection rule for one transition (a-b) is $\Delta M = 0$ and the other (c-d) is $\Delta M = \pm 1$. Clearly, off-resonant driving cannot occur in this case because the light is incorrectly polarized, and yet double resonances appear. The lines γ and δ are the primary three level resonances with a $\Delta M = 1$ interval in the lower and upper vibrational state respectively, and the lines α, β and ρ are the satellite four level resonances that are collision-induced.

4.4 Lamb-dip

Other experiments were conducted using one laser beam reflected back on itself through the Stark cell. With the selection rule $\Delta M = 0$ operating, this yields a series of Lamb-dips ($M = 1 \rightarrow 1$, $2 \rightarrow 2$, etc.) and

a set of lines, almost as intense, midway between them on a frequency scale. Thus, the double resonance condition $\Omega_1 = \frac{1}{2}(\omega_{ab} + \omega_{cd})$ is satisfied in agreement with Eq. (2.38). We see that a particular velocity group defined by Eq. (2.41) contains (1) molecules in level d that Doppler shift one light wave into resonance with the transition c-d, and (2) molecules in level b that Doppler shift the oppositely running light wave into resonance with transition a-b. Again, communication between the two transitions results from angular momentum tipping collisions that preserve velocity v_z. That such a coupling must occur is especially evident here since only one of the two light beams is monitored. However, in this case the Lamb-dip and satellite lines are observed to have the same line width in agreement with Eq. (2.37) and in contrast to the double resonance results of Section 4.1.

5. THE DIPOLE INTERACTION

The mechanism which tips the angular momentum vectors of two colliding CH_3F molecules is the long-range anisotropic interaction of their permanent electric dipoles.[9] We consider one of the molecules in state $|J,K,M\rangle$ and with velocity v_z to be tagged by the laser beam, and the other molecule is in an arbitrary state with any velocity. Due to the weakness of the interaction, the collision pair proceeds along nearly straight line trajectories without changing their rotational or vibrational energy. A small orientational or Stark energy is exchanged, however, for translational energy which modifies the average v_z component of each. This velocity smearing, which is on the order of 0.5% of thermal velocity, contributes to the satellite line width but as yet has not been detected

because of its smallness. These experiments, therefore, allow a detailed unfolding of the relaxation process in its dependence on J, K, and M quantum states as well as on v_z.

The dipole-dipole collision mechanism for two symmetric top molecules was originally discussed by Anderson[9] who showed that the relevant matrix elements are the same as for radiative transitions with selection rules $\Delta J = 0, \pm 1$, $\Delta M = 0, \pm 1$, and $\Delta K = 0$. To first order, the transition rate for one of the collision partners, when J is fixed, will be proportional to the matrix element squared

$$|\langle J,K,M|H_{dipole}|J,K,M\pm1\rangle|^2 \propto K^2(J\pm M+1)(J\mp M)/[J^2(J+1)^2] \qquad (5.1)$$

where

$$H_{dipole} = \left[\mu_1\cdot\mu_2 - 3\,\frac{(\mu_1\cdot r)(\mu_2\cdot r)}{r^2}\right]\Big/ r^3 \,. \qquad (5.2)$$

It is apparent that molecules with high J and low K are not tipped easily. This is in conformity with the classical argument that more rapidly rotating objects are more difficult to reorient by an external force. Only the component of the dipole moment μ along the J direction is fixed in orientation and can exert a time-averaged force on a second molecule where the projection of μ along J is $\mu \cos\theta = \mu K/J$, in accord with (5.1). It is for this reason that collision-induced double resonance has been seen here in the $^{13}CH_3F$ transition (J,K) = (4,3) → (5,3) but not in our earlier studies[8] of the $^{12}CH_3F$ transition (J,K) = (12,2) → (12,2). The

double-resonance spectrum for the latter is reproduced in Fig. 5 and shows no hint of satellite lines, particularly midway between the two primary three level resonances. Estimates based on (5.1) suggest that the satellite lines of Fig. 5 should be weaker than those in Figs. 1 and 4 by about two orders of magnitude. On the other hand, microwave double resonance experiments[24] failed to show any collision induced $\Delta M = \pm 1$ transitions (J constant) for OCS because for a linear molecule, the dipole direction is not fixed, corresponding to $K = 0$, and the time average force between two molecules is zero.

An estimate of the cross section for reorienting CH_3F collisions can be derived from the intensity ratio of lines (d) to (c) or (d) to (e) of Fig. 1. The intensity ratio of the satellite line, Eq. (2.34), to the primary line, (A.19), is just $(\kappa_{ac} + \kappa_{bd})/2 = \gamma'/\gamma$ when we take into account the difference in line widths and ignore power broadening. This gives $\gamma'/\gamma \cong 0.15$ and a cross section of $\sim 100 \text{Å}^2$ for $\Delta M = \pm 1$ collisions, as an average of the upper (J,K = 5,3) and lower (J,K = 4,3) vibrational states. We infer that the remaining 85% involves $\Delta J = \pm 1$ jumps; the matrix elements are also given by Anderson.[9]

The cross section is only an estimate. The lines c, d and e contain 7, 8 and 9 different transitions each. They are distributed over the Doppler profile and only an exact knowledge of their positions would allow a precision determination of the cross section.

By inspection of Table I, we see that lines (b) and (f) each involve a $\Delta M = 1$ and a $\Delta M = 3$ splitting whereas line (d) involves two $\Delta M = 1$ intervals. We see from Fig. 1 that lines (b) and (f) are indeed half as intense as (d) in agreement with the idea that $\Delta M = 1$ jumps are significantly more probable than $\Delta M = 3$ jumps, the result being approximately independent of vibrational state. Line (a) which is about one-fourth the intensity of (b) or (f) exhibits a $\Delta M = 4$ and $\Delta M = 2$ interval and requires either two $\Delta M = 1$ jumps in series (see Appendix D) or a single $\Delta M = 2$ jump. The selection rules that apply in this case will require further study as well as the behavior of CH_3F in the presence of foreign buffer gases where dipole-induced dipole and dipole-quadrupole interactions can occur.

APPENDIX A

THREE LEVEL DOUBLE RESONANCE

In Fig. 2(a) we label the top level a and the two lower levels b and d with the selection rules chosen so that

$$\langle a|\mu|b\rangle = \mu_{ab} \neq 0$$

$$\langle a|\mu|d\rangle = \mu_{ad} \neq 0 \ .$$

This is the case treated in detail by Feld and Javan.[7] We recalculate their result within the present framework to allow an easy comparison with the new features discussed in the present work. We consider a velocity group such that Ω_1 is nearly in resonance with ω_{ab} and Ω_2 with ω_{ad}. Like Ref. 7 we restrict our treatment to the case where E_2 is small enough to admit a perturbation treatment.

When $E_2 = 0$ we easily obtain the zeroth order solution (cf. Eqs. (2.14)-(2.16) with $\kappa = 0$)

$$\tilde{\rho}_{ab}^{(0)} = \frac{\alpha_1}{(\Delta_1 + kv) - i\gamma} n_{ba} \tag{A.1}$$

$$n_{ba}^{(0)} = \left(\frac{\lambda_b - \lambda_a}{\gamma}\right)\left[1 - 4\alpha_1^2 \frac{1}{(\Delta_1 + kv)^2 + \Gamma_1^2}\right] \ . \tag{A.2}$$

In addition, we need to solve the first order perturbation equations

$$i\dot{\rho}_{ad}^{(1)} = (\omega_{ad} - i\gamma)\rho_{ad}^{(1)} - 2\alpha_1 \cos(\Omega_1 t - kz)\rho_{bd}^{(1)} \tag{A.3}$$

$$i\dot{\rho}_{bd}^{(1)} = [-\omega_{db} - i\gamma]\rho_{bd}^{(1)} - 2\alpha_1 \cos(\Omega_1 t - kz)\rho_{ad}^{(1)}$$

$$+ 2\beta_2 \cos(\Omega_2 t - kz)\rho_{ba}^{(0)} \tag{A.4}$$

where we have expanded in

$$\beta_2 = \frac{\mu_{ad} E_2}{2\hbar} . \tag{A.5}$$

We introduce (2.13) and

$$\begin{aligned} \tilde{\rho}_{ad}^{(1)} &= \rho_{ad}^{(1)} e^{i(\Omega_2 t - kz)} \\ \tilde{\rho}_{bd}^{(1)} &= \rho_{bd}^{(1)} e^{-i\Delta\Omega t} \end{aligned} \tag{A.6}$$

where $\Delta\Omega = \Omega_1 - \Omega_2$. From (A.3)-(A.4) follows, in the rotating wave approximation,

$$[\Delta_3 + kv - i\gamma]\tilde{\rho}_{ad}^{(1)} = \alpha_1 \tilde{\rho}_{bd}^{(1)} + \beta_2 n_{da}^{(0)} \tag{A.7}$$

$$[\omega_{db} - \Delta\Omega + i\gamma]\tilde{\rho}_{bd}^{(1)} = -\alpha_1 \tilde{\rho}_{ad}^{(1)} + \beta_2 \tilde{\rho}_{ba}^{(0)} \tag{A.8}$$

where

$$n_{da}^{(0)} \equiv \rho_{dd}^{(0)} - \rho_{aa}^{(0)}$$

$$= \rho_{dd}^{(0)} - \frac{1}{2}\left(\rho_{aa}^{(0)} + \rho_{bb}^{(0)} - \rho_{bb}^{(0)} + \rho_{aa}^{(0)}\right)$$

$$= \rho_{dd}^{(0)} - \left(\frac{\lambda_b - \lambda_a}{\gamma}\right) \frac{2\alpha_1^2}{(\Delta_1 + kv)^2 + \Gamma_1^2} \qquad (A.9)$$

and

$$\Delta_3 = \omega_{ad} - \Omega_2 \, . \qquad (A.10)$$

Solving from (A.7) and (A.8) we obtain

$$\tilde{\rho}_{ad}^{(1)} = \beta_2 \frac{\left(\frac{\lambda_b - \lambda_a}{\gamma}\right) + \frac{\alpha_1}{\omega_{db} - \Delta\Omega + i\gamma} \tilde{\rho}_{ba}^{(0)}}{\Delta_3 + kv + \frac{\alpha_1^2}{\omega_{db} - \Delta\Omega + i\gamma} - i\gamma} \, . \qquad (A.11)$$

Inserting

$$\tilde{\rho}_{ba}^{(0)} = \frac{\alpha_1(\lambda_b - \lambda_a)/\gamma}{(\Delta_1 + kv)^2 + \Gamma_1^2} (\Delta_1 + kv - i\gamma) \qquad (A.12)$$

and $n_{da}^{(0)}$ from (A.9) we find

$$\tilde{\rho}_{ad}^{(1)} = -\beta_2 \alpha_1^2 \frac{1}{\left[\Delta_3 + kv + \frac{\alpha_1^2}{\omega_{db} - \Delta\Omega + i\gamma} - i\gamma\right][\Delta_1 + kv + i\Gamma_1]}$$

$$\times \left[\frac{2}{(\Delta_1 + kv - i\Gamma_1)} - \frac{(\Delta_1 + kv - i\gamma)}{(\Delta_1 + kv - i\Gamma_1)} \frac{1}{(\omega_{db} - \Delta\Omega + i\gamma)}\right] \left(\frac{\lambda_b - \lambda_a}{\gamma}\right) . \qquad (A.13)$$

Here the term proportional to $\rho_{dd}^{(0)}$ (cf. (A.9)) has been omitted as irrelevant for the double resonance phenomenon.

Performing the Doppler average of (A.13) we notice that the only singularity at the integrand in the lower half-plane is

$$kv = -\Delta_1 - i\Gamma_1 \tag{A.14}$$

and we can calculate

$$\left\langle \tilde{\rho}_{ad}^{(1)} \right\rangle_{vel} = \frac{\beta_2 \alpha_1^2}{ku\sqrt{\pi}} e^{-\Delta_1^2/k^2u^2}$$

$$\times (2\pi i) \frac{\omega_{db} - \Delta\Omega + i\gamma + \frac{1}{2} i(\gamma + \Gamma_1)}{i\Gamma_1\{[\omega_{db} - \Delta\Omega + i(\gamma + \Gamma_1)][\omega_{db} - \Delta\Omega + i\gamma] - \alpha_1^2\}} \left(\frac{\lambda_b - \lambda_a}{\gamma}\right) . \tag{A.15}$$

The zeroes of the denominator are

$$\omega_{db} - \Delta\Omega = -\frac{1}{2} i[(2\gamma + \Gamma_1) \pm \sqrt{\Gamma_1^2 - 4\alpha_1^2}]$$

$$= -\frac{1}{2} i(2\gamma + \Gamma_1 \pm \gamma) . \tag{A.16}$$

The singularity of width $\frac{3}{2}\gamma + \frac{1}{2}\Gamma_1$ cancels the numerator and we are left with

$$\left\langle \tilde{\rho}_{ad}^{(1)} \right\rangle_{vel} = \frac{2\sqrt{\pi}\ \beta_2 \alpha_1^{\,2}}{ku\Gamma_1} \frac{e^{-\Delta_1^{\,2}/k^2u^2}}{[\omega_{db} - \Delta\Omega + \frac{1}{2}\, i(\gamma + \Gamma_1)]} \frac{(\lambda_b - \lambda_a)}{\gamma} \,. \tag{A.17}$$

This is the narrow resonance obtained by Feld and Javan (Eq. (54) of Ref. 7).

As in Eqs. (2.32)-(2.34) we calculate the power absorbed by the sample

$$W = \frac{1}{2} N \left\langle \mu_{ab} E_1 \Omega_1 2\mathrm{Im}\tilde{\rho}_{ab}^{(1)} + \mu_{ad} E_2 \Omega_2 2\mathrm{Im}\tilde{\rho}_{ad}^{(1)} \right\rangle_{vel} \,. \tag{A.18}$$

We have calculated $\tilde{\rho}_{ad}^{(1)}$, and a similar calculation gives $\tilde{\rho}_{ab}^{(1)}$. We insert these into (A.18) and obtain

$$W = -\frac{2\sqrt{\pi}\ N\alpha_1^{\,2}\beta_2^{\,2}}{ku\Gamma_1\Gamma_2} e^{-(\Delta_1^{\,2}/k^2u^2)} \left[\frac{\Gamma_1(\gamma + \Gamma_2)}{(\omega_{db} - \Delta\Omega)^2 + \frac{1}{4}(\gamma + \Gamma_2)^2} \hbar\Omega_1 \left(\frac{\lambda_d - \lambda_c}{\gamma} \right) \right.$$

$$\left. + \frac{\Gamma_2(\gamma + \Gamma_1)}{(\omega_{db} - \Delta\Omega)^2 + \frac{1}{4}(\gamma + \Gamma_1)^2} \hbar\Omega_2 \left(\frac{\lambda_b - \lambda_a}{\gamma} \right) \right] \,. \tag{A.19}$$

This is the final result to be compared with the new double resonance (2.34).

APPENDIX B

EXTENSION OF THE COLLISION MODEL

The general collision kernel of Eq. (2.4)

$$\rho'(v) = \int \frac{dv'}{T(v')} \Pi(v,v')\rho(v') \tag{B.1}$$

mixes the velocity components. If we introduce this into Eq. (2.10) we get, instead of (2.17) (omitting the term $(\lambda_b - \lambda_a)/\gamma$),

$$\tilde{\rho}_{ab} - \tilde{\rho}_{ba} = \frac{2i\alpha_1}{(\Delta_1 + kv)^2 + \Gamma_1^2} \int \frac{\Pi(v,v')}{T(v')} \; n_{dc}(v')dv' \; . \tag{B.2}$$

Introducing the collisionless result (2.23) for n_{dc} we obtain (cf. (2.28))

$$\tilde{\rho}^{(1)}_{ab} - \tilde{\rho}^{(1)}_{ba} = - \frac{8i\alpha_1\alpha_2^2}{[(\Delta_1 + kv)^2 + \Gamma_1^2]} \int \frac{\Pi(v,v')}{\gamma T(v')} \frac{[\lambda_d(v') - \lambda_c(v')]}{[(\Delta_2 + kv')^2 + \Gamma_2^2]} dv' \tag{B.3}$$

and the observed quantity (2.32) will contain a term

$$W_+ = -8N\hbar\Omega_1\alpha_1^2\alpha_2^2 G(\Delta_1,\Delta_2) \tag{B.4}$$

where

$$G(\Delta_1,\Delta_2) = \int \frac{dv}{[(\Delta_1 + kv)^2 + \Gamma_1^2]} \int \frac{dv'}{\gamma T(v')} \Pi(v,v') \; \frac{[\lambda_d(v') - \lambda_c(v')]}{[(\Delta_2 + kv')^2 + \Gamma_2^2]} \tag{B.5}$$

We assume a Gaussian steady state distribution

$$\lambda_d(v) - \lambda_c(v) = \frac{\Delta\lambda}{\sqrt{\pi}\,u} e^{-v^2/u^2} \tag{B.6}$$

with a width $u >> \Gamma/k$. Then, $(\lambda_d - \lambda_c)$ can be taken outside the integral with $v' = \Delta_2/k$.

If we choose the collision kernel Π to be a symmetric function of an arbitrary linear combination of the velocities

$$\Pi(v,v') = \Pi(v - \alpha v') \tag{B.7}$$

we find

$$\begin{aligned} \langle v \rangle &= \int v\Pi(v,v')dv \\ &= \alpha v' \end{aligned} \tag{B.8}$$

which shows that the center of gravity of the velocity distribution after the collision is $\alpha v'$ (this α should not be confused with α_1 and α_2). If $\alpha = 0$ we have complete randomization and if $\alpha = 1$ we have a distribution symmetric around the velocity before the collision. The width of the distribution is

$$\langle (v - \langle v \rangle)^2 \rangle = \int v^2\Pi(v,v')dv - \langle v \rangle^2 \equiv \Delta u^2 \ . \tag{B.9}$$

A kernel of this type is the Keilson-Storer[25] collision kernel where

$$\Pi(v,v') = \left(\frac{\beta}{\pi}\right)^{1/2} e^{-\beta(v-\alpha v')^2} . \qquad (B.10)$$

In Ref. 25 it is shown that the kernel (B.10) leads to the thermal equilibrium (B.6) in the absence of radiation if

$$\beta = \frac{1}{(1 - \alpha^2)u^2} \qquad (B.11)$$

which gives for (B.9)

$$\Delta u^2 = \frac{1}{2} (1 - \alpha^2)u^2 . \qquad (B.12)$$

For $\alpha = 0$ this shows that we regain the thermal distribution (B.6) from (B.1) with the width $\frac{1}{2} u^2$. When α approaches one (velocity persists) (B.12) shows that Δu becomes small and the velocity distribution narrows.

Already the general form (B.7) allows us to draw several conclusions about the distribution in Δ_1, Δ_2. Assuming T to be independent of velocity (slowly varying over a range $v \simeq \Gamma/k$) and changing to the variables $x = kv$, $y = kv'\alpha$ we find

$$G(\Delta_1,\Delta_2) = \frac{\Delta\lambda}{\gamma T} \frac{\alpha}{k^2\sqrt{\pi}u} \int \frac{dx}{[(\Delta_1+x)^2 + \Gamma_1^2]} \int dy\ \Pi\left(\frac{x-y}{k}\right) \frac{\exp[-(y/(\alpha ku))^2]}{[(\alpha\Delta_2+y)^2 + \alpha^2\Gamma_2^2]} \qquad (B.13)$$

Because Π is a symmetric function we can see that the distribution $G(\Delta_1,\Delta_2)$ has a maximum for $\Delta_1 = \alpha\Delta_2$ which gives

$$\Omega_1 - \Omega_2 = \omega_{ab} - \omega_{cd} - (1 - \alpha)\Delta_2 \ . \qquad (B.14)$$

The resonance is thus shifted by $(1 - \alpha)\Delta_2$ which is small in the cases under consideration (perhaps 10^2 Hz). Measuring both beams as in (2.26) one finds no shift but a broadening as the term in field 2 is shifted to

$$\Omega_1 - \Omega_2 = \omega_{ab} - \omega_{cd} + (1 - \alpha)\Delta_1 \qquad (B.15)$$

which goes in the opposite direction. This result is obtained in the same way as above. When there is little spread in the velocity by a collision we set

$$\Pi(\Delta v) = \delta(\Delta v) \qquad (B.16)$$

and (B.4)-(B.5) reproduces the result (2.34). The width of the line is then $\Gamma_1 + \Gamma_2$. The total width Γ_t of the distribution (B.13) is of order

$$\Gamma_t^{\,2} = (\Gamma_1 + \alpha\Gamma_2)^2 + k^2\Delta u^2 \qquad (B.17)$$

where we used (B.9). We have taken the widths of the Lorentzians to add linearly, which in the limit (B.16) reproduces (2.34) correctly, and combined it quadratically with the velocity-changing collision contribution.

From the observed line widths Γ_t, Γ_1 and Γ_2 ($\alpha \approx 1$), the quantity $k\Delta u$ in (B.17) could be obtained (see Section 4.1). To obtain more detailed

information about the kernel Π one would have to deconvolute (B.5). In the limit of large collisional velocity transfer

$$k\Delta u >> \Gamma_{1,2} \tag{B.18}$$

we obtain from (B.5)

$$G(\Delta_1,\Delta_2) = \frac{\pi^{3/2}}{\Gamma_1\Gamma_2}\frac{\Delta\lambda}{\gamma T u k^2}\,\Pi\left(\frac{\Delta_1}{k}\,,\,\frac{\Delta_2}{k}\right)e^{-(\Delta_2/ku)^2} \tag{B.19}$$

which shows that, in this limit, the tuning spectrum as a function of Δ_1 and Δ_2 gives Π directly. In practical cases (B.18) may well be satisfied even when $k\Delta u$ is much less than the Doppler width. The measurements by Rhodes et al.[13] are closer to this regime than the present work.

APPENDIX C

OFF-RESONANT DRIVING MECHANISM

Another process that has been considered as the cause of the double resonance phenomenon will be discussed here.

We consider the field $E_2 e^{i(\Omega_2 t - kz)}$, where $z = z_o + v(t - t_o)$, acting on molecules with a velocity that is in resonance with the transition c-d. The induced dipole moment is then

$$\tilde{\rho}_{cd} \equiv e^{i(\Omega_2 t - kz)} \rho_{cd} = \frac{\alpha_2}{(\Delta_2 + kv) + i\gamma} n_{cd} . \tag{C.1}$$

The same field can, however, drive another transition a-b in an off-resonant fashion. To consider this we write down a correction $\rho_{ab}^{(1)}$ to the polarization of the transition a-b driven by the field E_2, viz.

$$i\dot{\rho}_{ab}^{(1)} = (\omega_{ab} - i\gamma)\rho_{ab}^{(1)} - 2\alpha_2' \cos(\Omega_2 t - kz) n_b^{(0)} \tag{C.2}$$

where

$$\alpha_2' = \frac{\mu_{ab} E_2}{2\hbar} = \frac{\mu_{ab}}{\mu_{cd}} \alpha_2 . \tag{C.3}$$

Introducing the ansatz

$$\rho_{ab}^{(1)} = \tilde{\rho}_{ab}^{(1)} e^{-i(\Omega_2 t - kz)} \tag{C.4}$$

we find from (C.2)

$$\tilde{\rho}_{ab}^{(1)} = \frac{\alpha_2'}{\Delta_1 + kv + \Delta\Omega + i\gamma}\left(\frac{\lambda_b - \lambda_a}{\gamma}\right) \qquad (C.5)$$

where $\Delta\Omega = \Omega_1 - \Omega_2$. If now the field $E_1 e^{i(\Omega_1 t - kz)}$ drives the same velocity group at resonance we can insert

$$n_{ba}^{(0)} = \left(\frac{\lambda_b - \lambda_a}{\gamma}\right)\left[1 - \frac{4\alpha_1^2}{(\Delta_1 + kv)^2 + \gamma^2}\right] , \qquad (C.6)$$

where only the second term will be of interest. The total dipole moment oscillating at the frequency Ω_2 is now

$$P_2 = N\int dv[\mu_{ab}\tilde{\rho}_{ab}^{(1)}(v)\ e^{-ikvt} + \mu_{cd}\tilde{\rho}_{cd}^{(0)}(v)\ e^{-kvt}] . \qquad (C.7)$$

This polarization will radiate by Maxwell's equations and in the radiated energy there will be a cross term corresponding to

$$W \propto \mathrm{Re}\iint \tilde{\rho}_{cd}^{(0)}(v)^*\tilde{\rho}_{ab}^{(1)}(v')e^{ik(v-v')t}\ dvdv' . \qquad (C.8)$$

This quantity will be time independent only when $v' = v$ and interferes destructively otherwise. The electromagnetic wave is scattered off two molecular groups (in different level pairs) and the forward scattered radiation interferes destructively except when the two groups have the same velocity. The observed quantity is then from (C.5)-(C.7)

$$W \propto \mathrm{Re} \int (\tilde{\rho}_{cd}^{(0)}(v))^{*} \tilde{\rho}_{ab}^{(1)}(v)dv = -\left(\frac{(\lambda_c - \lambda_d)(\lambda_b - \lambda_a)}{\gamma^2}\right) 4\alpha_2\alpha_2' \alpha_1^2$$

$$\times \iint \frac{1}{[(\Delta_1 + kv + \Delta\Omega + i\gamma)]} \frac{1}{[(\Delta_2 + kv) + i\gamma]} \left(\frac{dv}{(\Delta_1 + kv)^2 + \gamma^2}\right)$$

$$\approx - \frac{4(\lambda_c - \lambda_d)(\lambda_b - \lambda_a)\alpha_1^2\alpha_2^2}{\gamma^2\Delta\Omega}$$

$$\times \int dv \frac{(\Delta_2 + kv)}{[(\Delta_1 + kv)^2 + \gamma^2][(\Delta_2 + kv)^2 + \gamma^2]} \qquad (C.9)$$

where we have noted that $\Delta\Omega >> (\Delta_1 + kv) \lesssim \gamma$. Performing the integral we obtain

$$W \propto - \frac{4\pi(\lambda_c - \lambda_d)(\lambda_b - \lambda_a)\alpha_1^2\alpha_2^2}{\gamma^3\Delta\Omega} \frac{(\Delta_2 - \Delta_1)}{[(\Delta_2 - \Delta_1)^2 + 4\gamma^2]} . \qquad (C.10)$$

We observe that this result involves the following features:

(a) It occurs in the order $\alpha_1^2\alpha_2^2$ like the other double resonance phenomena.

(b) It shows a resonant behavior for $\Delta_1 = \Delta_2$ as the result (2.34).

(c) It has twice the width (2γ) of the ordinary double resonance (Let $\Gamma_1 = \gamma$ in (A.19)).

(d) It shows a dispersive behavior near resonance due to the $\Delta_2 - \Delta_1$ in the numerator.

(e) Because of the factors $(\lambda_c - \lambda_d)(\lambda_b - \lambda_a)$, the effect is expected to depend quadratically on pressure.

The experimentally observed resonances agree with features (a)-(c) but clearly disagree with (d). Experiments also show a more complicated pressure dependence than the single quadratic dependence of (e). This can be explained by the collisional coupling, which involves pressure in a more essential way, see Section 5. Finally, an estimate of the contributions from processes of the type (C.10) indicates that they should be at least three orders of magnitude too weak to be observed in the present experiments. It, hence, appears as if this mechanism can be dismissed as an explanation of the new resonances.

APPENDIX D

SEQUENTIAL TRANSFER OF POPULATIONS

We now assume that the transition b→d in Fig. 2(b) occurs via an intermediate level e through two collision processes, each collision obeying the $\Delta M = \pm 1$ selection rule. As we are investigating a velocity group such that Ω_1 resonates with a-b and Ω_2 with c-d, it is not possible for $|e\rangle$ to be in resonance with either field. (We assume the splitting between the sublevels to greatly exceed the power broadened line width. This is satisfied in the experiments.) Thus we obtain the equation for the population of $|e\rangle$

$$\frac{\partial \rho_{ee}}{\partial t} = -\gamma_e \rho_{ee} + \gamma_e \kappa_{be} \rho_{bb} + \gamma_e \kappa_{ed} \rho_{dd} \cdot \tag{D.1}$$

In steady state we find

$$\rho_{ee} = \kappa_{be} \rho_{bb} + \kappa_{ed} \rho_{dd} \cdot \tag{D.2}$$

For the population of level $|b\rangle$ we thus obtain

$$\frac{\partial \rho_{bb}}{\partial t} = -\gamma_b \rho_{bb} + \gamma_b \kappa_{be} \rho_{ee} + \text{radiative terms}$$

$$= -\gamma_b (1 - \kappa_{be}^2) \rho_{bb} + \gamma_b \kappa_{be} \kappa_{ed} \rho_{dd} + \ldots \tag{D.3}$$

Comparing this equation with Eq. (2.10) we find that the factor $(1 - \kappa_{be}^2)$ is to be incorporated into the effective decay rate γ and the coupling to level $|d\rangle$ is given (to lowest order in the collision fraction κ) by

$$\kappa_{bd} = \kappa_{be}\kappa_{ed} \cdot \tag{D.4}$$

This is a natural result which can straightforwardly be extended to higher order sequential couplings. The coupling (D.4) will exhibit a different pressure behavior from the case where the levels are coupled by a single collision. If we also have a single collision coupling κ'_{bd} between b and d, we obtain for the total coupling b-d the expression

$$(\kappa_{bd})_{total} = \kappa'_{bd} + \kappa_{be}\kappa_{ed} \cdot \tag{D.5}$$

Because the present experimental method allows separate measurements of the different resonances, one can separately measure $\kappa_{be}\kappa_{ed}$ and $(\kappa_{bd})_{total}$. From this κ'_{bd} can be deduced.

For example line (a) in Fig. 1 consists of levels differing by $\Delta M = 2$ and $\Delta M = 4$. Assuming the coupling between $\Delta M = 4$ levels to be negligible, the sequential decay rate $(\kappa_{\Delta M=1})^2$ can be determined from the resonances (b), (d) and (f) (see Section 5) and if the intensity of (a) were known accurately, (D.5) would give κ', i.e., the amount of single collision mixing for levels separated by $\Delta M = 2$. This would derive from either a second order Born approximation or a breakdown of the dipole selection rules in a collision. This indicates a type of experiment that is made possible by the new double resonances, but for the moment the intensity of (a) is too weak to allow any specific conclusions.

REFERENCES

1. V. W. Hughes and L. Grabner, Phys. Rev. 79, 314 (1950); P. Kusch and V. W. Hughes, Encyclopendia of Physics, Vol. XXXVII/1 (Springer-Verlag, Berlin, 1959), Sec. 30.

2. J. Brossel, P. Sagalyn and F. Bitter, Phys. Rev. 79, 225 (1950); J. Brossel and F. Bitter, Phys. Rev. 86, 308 (1952).

3. R. G. Brewer, R. L. Shoemaker and S. Stenholm, Phys. Rev. Lett., July 8, 1974.

4. W. E. Lamb, Jr., Phys. Rev. 134, A1429 (1964).

5. K. Shimoda, Double Resonance Spectroscopy of Molecules Using Lasers; Topics in Applied Physics, Volume II (Springer-Verlag, to be published), edited by H. Walther.

6. I. M. Beterov and V. P. Chebotaev, Progress in Quantum Electronics, edited by J. H. Sanders and S. Stenholm (Pergamon, Oxford 1974), Vol. 3, Part 1.

7. M. S. Feld and A. Javan, Phys. Rev. 177, 540 (1969).

8. (a) R. G. Brewer, Phys. Rev. Lett. 25, 1639 (1970); (b) R. G. Brewer, Science 178, 247 (1972).

9. P. W. Anderson, Phys. Rev. 76, 647 (1949).

10. J. Schmidt, P. R. Berman and R. G. Brewer, Phys. Rev. Lett. 31, 1103 (1973).

11. T. Oka, Advances in Atomic and Molecular Physics, Volume 9, p. 127 (Academic Press, New York, 1973), edited by D. R. Bates.

12. S. M. Freund, J. W. C. Johns, A. R. McKellar and T. Oka, J. Chem. Phys. 59, 3445 (1973).

13. T. W. Meyer and C. K. Rhodes, Phys. Rev. Lett. 32, 637 (1974).

14. It is easily seen that keeping $k_1 \neq k_2$ introduces correction terms $\propto(\Omega_1 - \Omega_2)(v/c)$.

15. S. Stenholm, Phys. Rev. A2, 2089 (1970).

16. W. R. Hindmarsh and J. M. Farr, Progress in Quantum Electronics, edited by J. H. Sandars and S. Stenholm (Pergamon, Oxford 1972), Vol. 2, Part 3.

17. Remember that $\dot{\rho} = \frac{\partial \rho}{\partial t} + v \frac{\partial \rho}{\partial z}$ because of the time dependence of the molecular position.

18. C. Freed, IEEE J. Quantum Electron 4, 404 (1968) and 3, 203 (1967); the design is similar to that described in this reference.

19. W. L. Smith and I. M. Mills, J. Mol. Spectroscopy 11, 11 (1963).

20. R. G. Brewer, M. J. Kelly and A. Javan, Phys. Rev. Lett. 23, 559 (1969).

21. C. H. Townes and A. L. Schawlow, Microwave Spectroscopy (McGraw-Hill, New York, 1955).

22. S. C. Wofsy, J. S. Muenter and W. Klemperer, J. Chem. Phys. 55, 2014 (1971).

23. S. M. Freund, G. Duxbury, M. Römheld, J. T. Tiedje and T. Oka (to be published).

24. A. P. Cox, G. W. Flynn and E. B. Wilson, Jr., J. Chem. Phys. 42, 3094 (1965); M. Unland and W. H. Flygare, J. Chem. Phys. 45, 2421 (1966).

25. J. Keilson and J. E. Storer, Quart. Appl. Math. 10, 243 (1952).

Table I: $^{13}CH_3F$ Double Resonance Lines ($\Delta\Omega$ = 30.008 MHz)*

Line	Stark Tuning Rate ($kHz \cdot volts^{-1} \cdot cm$)	Line Center ($volts \cdot cm^{-1}$)		Line Width (kHz, FWHM)
		observed	predicted	
a	370.9 $(4\Delta_\ell - 2\Delta_u)$	80.90	80.78	960
b	326.2 $(3\Delta_\ell - \Delta_u)$	92.00	91.85	640
c	281.99$(2\Delta_\ell)$	106.42	106.42	410
d	237.0 $(\Delta_\ell + \Delta_u)$	126.58	126.51	810
e	192.48$(2\Delta_u)$	155.90	155.90	400
f	147.8 $(3\Delta_u - \Delta_\ell)$	203.08	203.17	750

*Selection rules: $\Delta M = \pm 1$ in both transitions. See Fig. 1.

Table II: $^{13}CH_3F$ Double Resonance Lines ($\Delta\Omega$ = 40.039 MHz)*

Line	Stark Tuning Rate ($kHz \cdot volts^{-1} \cdot cm$)	Line Center ($volts \cdot cm^{-1}$)		Line Width (kHz, FWHM)
		observed	predicted	
b	325.6 $(3\Delta_\ell - \Delta_u)$	122.98	122.93	440
c	281.07$(2\Delta_\ell)$	142.45	142.45	250
d	236.4 $(\Delta_\ell + \Delta_u)$	169.36	169.34	495
e	191.82$(2\Delta_u)$	208.73	208.73	240
f	147.1 $(3\Delta_u - \Delta_\ell)$	272.12	272.01	590

*Selection rules: $\Delta M = \pm 1$ in both transitions.

Table III: CH_3F Dipole Moment (in Debye)

v_3,J,K	$^{13}CH_3F$	v_3,J,K	$^{12}CH_3F$ (Ref. 8(b))
0,4,3	1.8578(6)	0,12,2	1.8597(4)
1,5,3	1.9038(6)	1,12,2	1.9067(4)

Table IV: $^{13}CH_3F$ Double Resonance Lines ($\Delta\Omega$ = 29.930 MHz)*

Line	Stark Tuning Rate ($kHz \cdot volts^{-1} \cdot cm$)	Line Center ($volts \cdot cm^{-1}$)	
		observed	predicted
α	228.4 $(3\Delta_\ell - 2\Delta_u)$	131.0	130.4
β	184.5 $(2\Delta_\ell - \Delta_u)$	162.3	161.8
γ	140.35(Δ_ℓ)	213.25	213.25
δ	95.72(Δ_u)	312.68	312.68
ρ	51.52$(2\Delta_u - \Delta_\ell)$	580.9	585.8

*Selection rules: $\Delta M = 0$ in one transition and $\Delta M = \pm 1$ in the other.

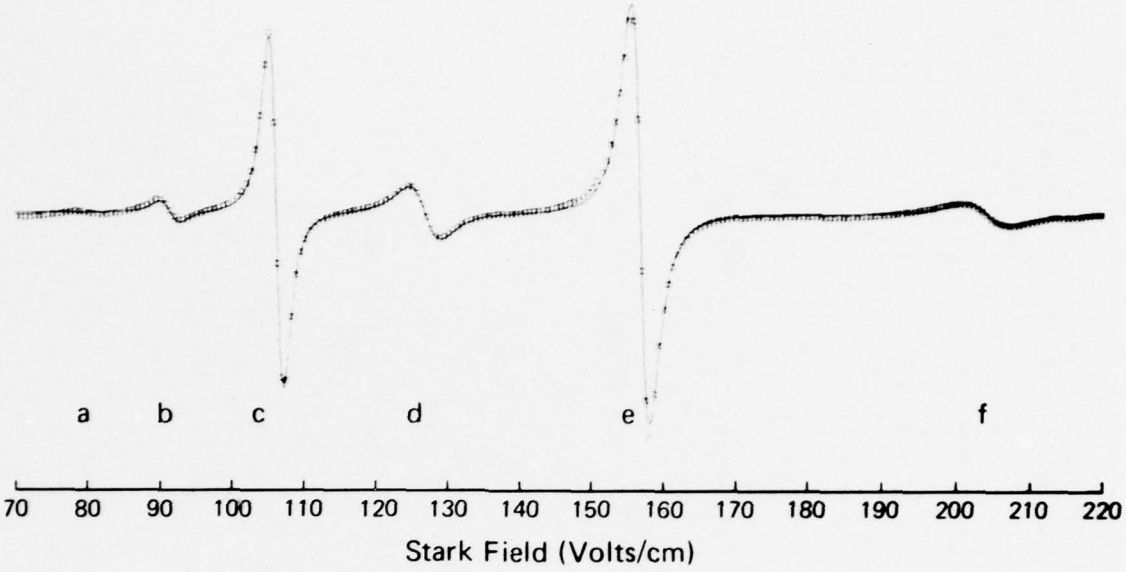

Figure 1. Optical double resonance spectrum for $^{13}CH_3F$ at ~3 m Torr pressure and $\Omega_1 - \Omega_2 = 30.008$ MHz. The optical selection rule is $\Delta M = \pm 1$. Lines (c) and (e) correspond to the level configuration of Fig. 2(a) and the others to Fig. 2(b). The Stark sweep is computer driven in steps and the output signal is digitized (squares) and least squares fitted to Lorentzian lineshapes (solid line). The Stark gap spacing is 0.60256 cm and the sample path length is 10 cm. (From Brewer et al., Ref. 3.)

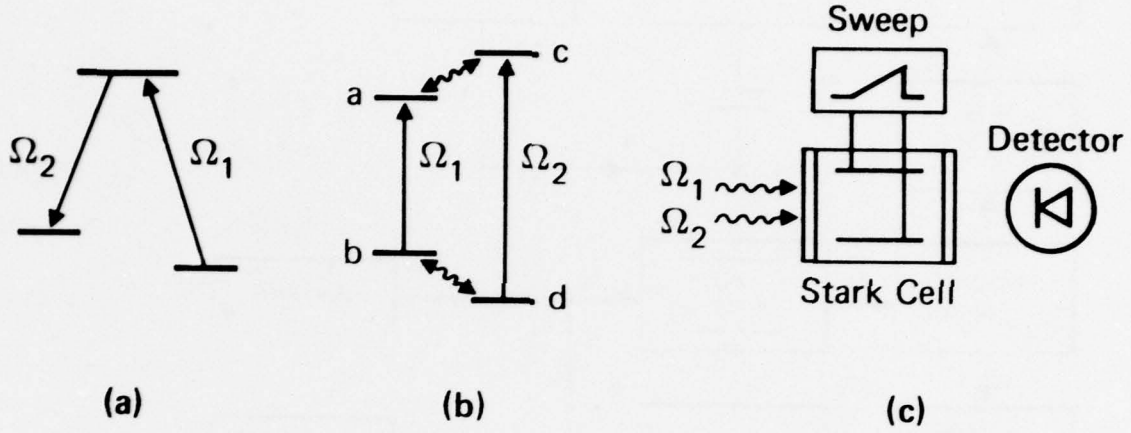

Figure 2. (a) Traditional double resonance level configuration; (b) Collision–induced double resonance level configuration; wavy lines indicate collision–induced transitions; (c) Experimental arrangement for monitoring optical double resonance signals.

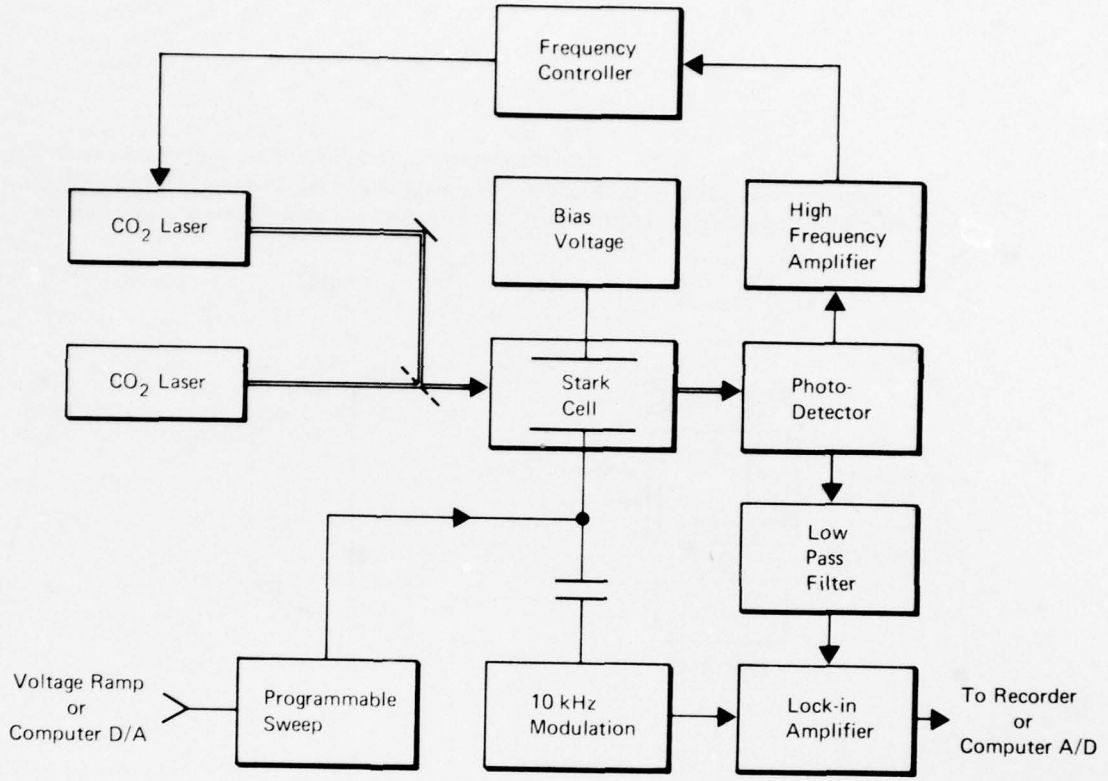

Figure 3. Block diagram of the double resonance experiment.

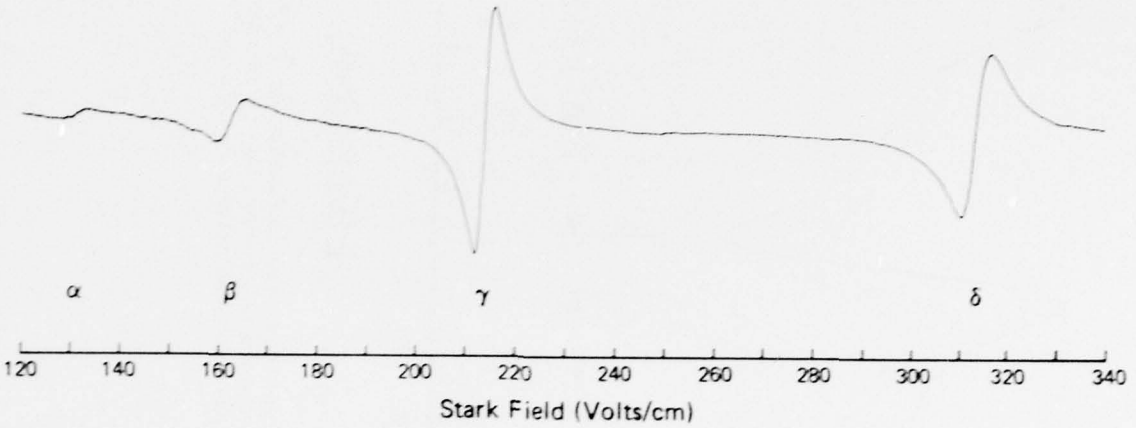

Figure 4. Optical double resonance spectrum for $^{13}CH_3F$ with $\Omega_1 - \Omega_2 = 29.930$ MHz. The optical selection rule is $\Delta M = 0$ for one transition and $\Delta M = \pm 1$ for the other. The spectrum is displayed directly on an $x-y$ recorder as the Stark field is swept continuously. The phase of the detector is reversed by π from Fig. 1. Lines γ and δ correspond to the level structure of Fig. 2(a) and α and β to Fig. 2(b).

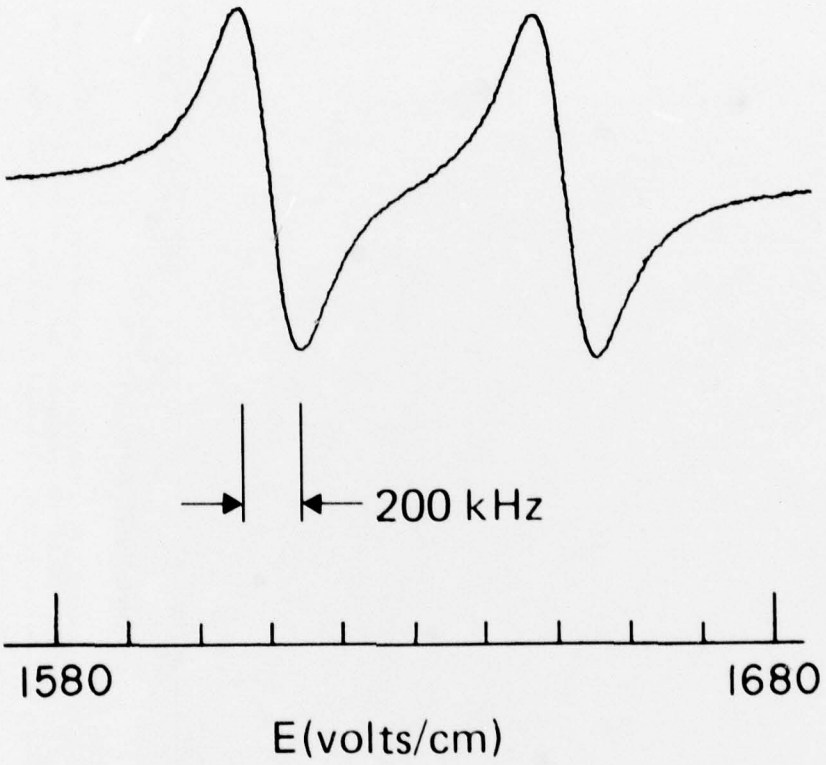

Figure 5. Optical double resonance spectrum for $^{12}CH_3F$ with $\Omega_1 - \Omega_2 = 39.629$ MHz. The optical selection rule is $\Delta M = \pm 1$. (See Ref. 8 for details.) The lines correspond to the level structure of Fig. 2(a).